Electronic Supplementary Material (ESI) for Physical Chemistry Chemical Physics.

Cation-π Aggregation-induced White Emission of Moisture-Resistant Carbon Quantum Dots: A Comprehensive Spectroscopic Study

Arman Ghasedi, Ehsan Koushki*, Javad Baedi

Department of Physics, Faculty of Sciences, Hakim Sabzevari University, Sabzevar, 96179-76487, Iran

* Corresponding author: E-mail: ehsan.koushki@yahoo.com, ehsan.koushki@hsu.ac.ir, Tel: +985144013164 (E. Koushki)

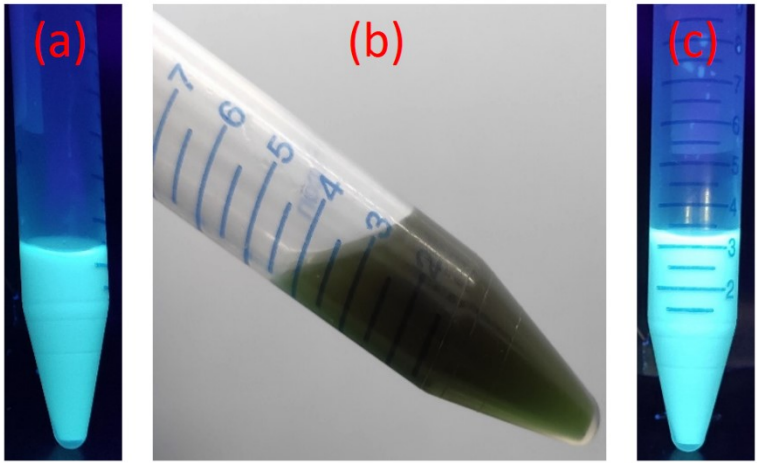

Figure S1. B-CQDs sample before the addition of NaOH under Uv irradiation (a), after addition of NaOH in daylight (b), and blue emission resulted upon adding NaOH under Uv illumination (c).

Figure S2. Light green emission from G-CQDs sample excited by 365 nm Uv lamp after the salting-out process.

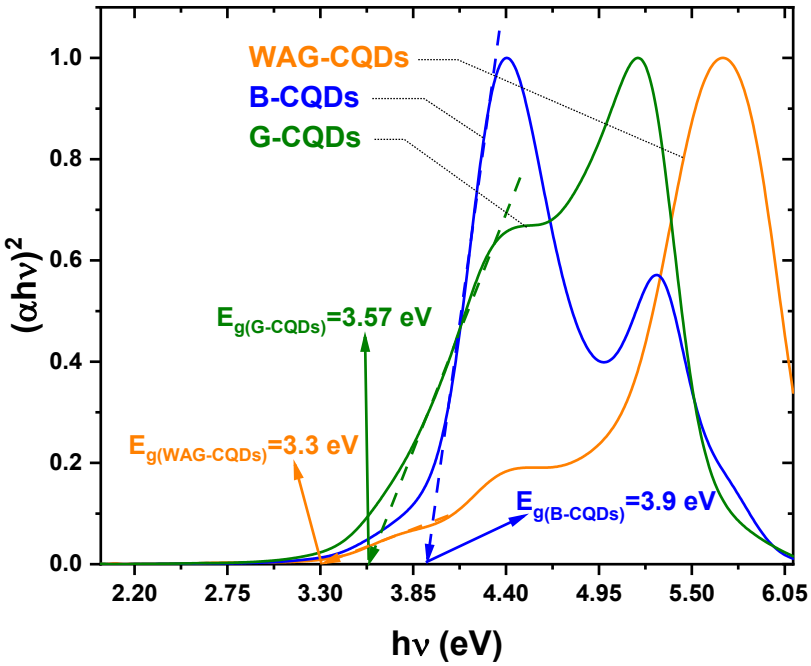

Figure S3. The calculated optical bandgap energies using Tauc's equation for WAG-, B-, and G-CQDs. The detail about the procedure of Tauc's equation implementation is presented below.

Tauc plot: The absorption coefficient (α) is related to photon energy ($h\upsilon$) by:

$$(\alpha h\upsilon)^{1/m} = \beta(h\upsilon - E_g)$$

where m, β, and E_g are transition mode factor, the band tailing parameter, and the energy of the optical bandgap. In the case of CQDs, the transition factor should be considered 1/2 due to direct gap nature of this material. According to Tauc's relation, plotting $(\alpha h\upsilon)^2$ versus the photon energy ($h\upsilon$) gives a straight line in a certain region. The extrapolation of this straight line will intercept the ($h\upsilon$) axis to give the value of the indirect optical energy gap (E_g).

Table S1. FTIR peak assignments

Sample	Frequency (cm^{-1})	Assigned vibration	Ref.
B-CQDs	3490	ν C-OH, COOH and H_2O	[1, 2]
	2930	ν_{as}C-H	[3]
	1650	ν C=O: ketones and 1,3-benzoquinones	[1, 2]
	1490-1580	ν_{as} C=C carboxylate	[4]
	1390	ν C-O	[1, 2]
	1250	τ C-H (CH_2twisting vibrations)/C-S and ω C-H (CH_2wagging vibrations)	[5, 6]
	1100	C-O axial stretching, alcohols	[7]
	1050	ν C-O	[8]
	879	ν C-O-C	[9]
	766	ν C-O: ethers and γ-butyrolactones	[9]
	661	ν C-H	[10]
G-CQDs	3520	ν C-OH, COOH and H_2O	[1, 2]
	2970	ν_{as}C-H	[3]
	1730	ν C=O: carboxyls (COOH) and/or scissor modes of H_2O	[1, 2]
	1590	ν_{as}C=C: in-plane asymmetric stretching of sp^2-hybridized C=C overlaps with C=O vibrations of ketones and 1,3-benzoquinones	[1]
	1510	ν_{as}C=C	[1]
	1370	ν C-O	[1, 2]
	1260	τ C-H/C-S and ω C-H	[5, 6]
	1170	ν C-O stretching vibration	[1, 2, 11]
	1090	ν C-C and ρ C-H (CH_2rocking vibrations)	[6]
	1040	ν C-O	[8]
	926	ρ C-H and ν C-C	[6]
	879	ν C-O-C	[9]

	835	ν C-O-C	[9]
	756	ν C-O: ethers and γ-butyrolactones	[9]
	692	ν C-O: mostly γ-butyrolactones groups	[9]
	580	ν C-H	[10]
	538	ν C-H	[12]
WAG-CQDs	3370	ν C-OH, COOH and H_2O	[1, 2]
	1740	ν C=O: carboxyls (COOH) and/or scissor modes of H_2O	[1, 2]
	1610	ν C=O	[1, 9]
	1590	ν_{as}C=C: in-plane asymmetric stretching of sp^2-hybridized C=C overlaps with C=O vibrations of ketones and 1,3-benzoquinones	[1]
	1510	ν_{as}C=C	[1]
	1470	ν_{as}C=C: in-plane asymmetric stretching of sp^2-hybridized C=C overlaps with C=O vibrations of ketones and 1,3-benzoquinones	[1]
	1260	τ C-H/C-S and ω C-H	[5, 6]
	1170	ν C-O stretching vibration	[1, 2, 11]
	1120	τ C-H and ω C-H	[5, 6]
	1020	ν C-O, ν C-C and ρ C-H	[1, 2]
	928	ρ C-H and ν C-C	[6]
	835	ν -O-: edge groups	[9]
	756	ν C-O: ethers and γ-butyrolactones	[9]
	729	ν C-O: mostly ethers	[9]
	694	ν C-O: ethers and γ-butyrolactones	[9]
	584	ν C-H	[10]

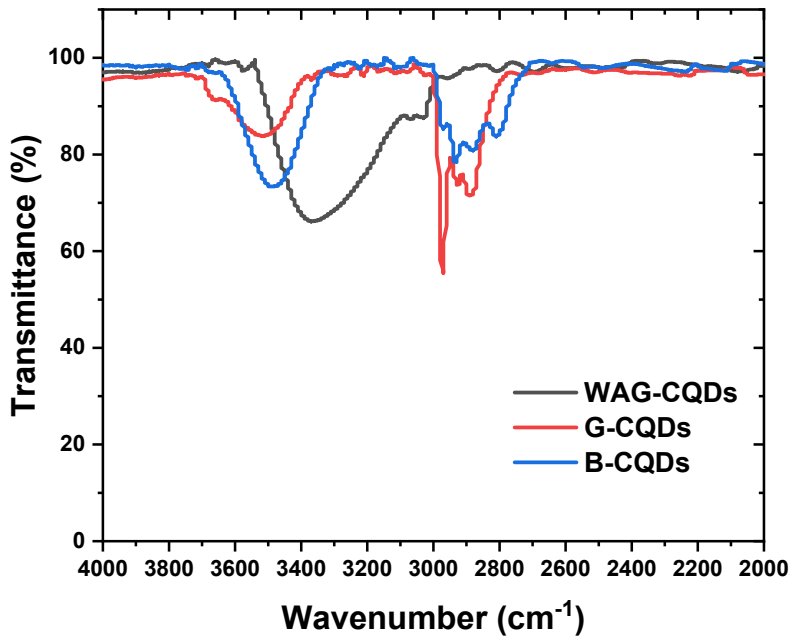

Figure S4. –OH band shift through aggregation.

Table S2. Characteristics and peak assignments of fitted Raman bands Ref. [13].

Sample	Raman bands (cm^{-1})						Intensity ratios				
	D1	D2	D	D3	G	D'	$\frac{I_D}{I_G}$	$\frac{I_{D1}}{I_G}$	$\frac{I_{D2}}{I_G}$	$\frac{I_{D3}}{I_G}$	$\frac{I_{D'}}{I_G}$
B-CQDs	-	1276	1357	1517	1595	1735	1.31	-	0.61	0.68	0.15
G-CQDs	1125	1263	1370	1513	1591	1677	1.81	0.41	0.93	0.65	0.05
WAG-CQDs	1113	1230	1307	1471	1600	1674	1.99	0.77	0.27	0.87	1.14
Peak assignment	sp^2-sp^3 carbon domains/ C-S	COOH/C -OH/S-O	Zig-zag/armchair states	C=O/ C-O	C=C	Crystalline defects					

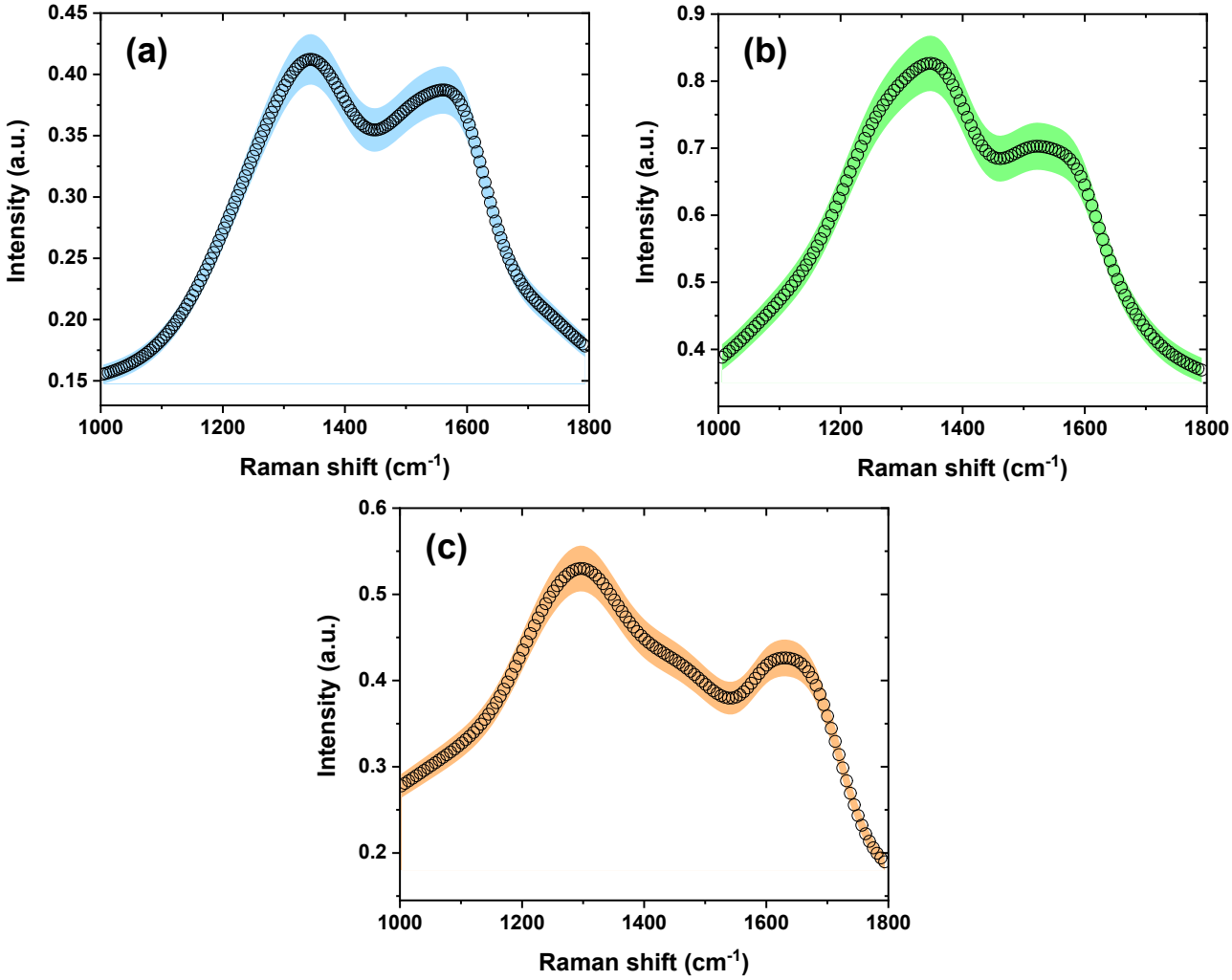

Figure S5. Calculated error bars (highlighted regions) for Raman spectra of B-CQDs (a), G-CQDs (b), and WAG-CQDs (c).

Table S3.The parameters and peak assignments of the deconvoluted PL peaks Ref. [13].

Sample (λ_{ex}=365 nm)	**Peak position (nm)**						
	P'	P0	P1	P2	P3	P4	P5
B-CQDs	-	-	422	458	-	-	621
G-CQDs	-	-	422	464	498	527	589
WAG-CQDs	367	416	431	446	-	-	618
Origin of the emissions	Intrinsic C emissions	C(=O)OH/zig-zag edge states	C-O-C	Armchair edge states/S containing doped sites	COOH/C-OH	C=O/C-O	Defect related emissions

Table S4. characteristics and peak assignments of the deconvoluted PL peaks of WAG-CQDs sample under different excitation wavelengths. Ref. [11, 13].

sample	**Peak position (nm)**						
	P'	P0	P1	P2	P3	P4	P5
WAG-CQDs λ_{ex}=300	-	407	437	455	-	-	620
WAG-CQDs λ_{ex}=365	367	416	431	431	-	-	618
WAG-CQDs λ_{ex}=400	367	416	-	446	482	-	590
WAG-CQDs λ_{ex}=420	-	403	429	459	496	527	588
Origin of the emissions	Intrinsic C emissions	C(=O)OH/ zig-zag edge states	C-O-C	Armchair edge states/S containing doped sites	COOH/C -OH	C=O/C -O	Defect related emissions

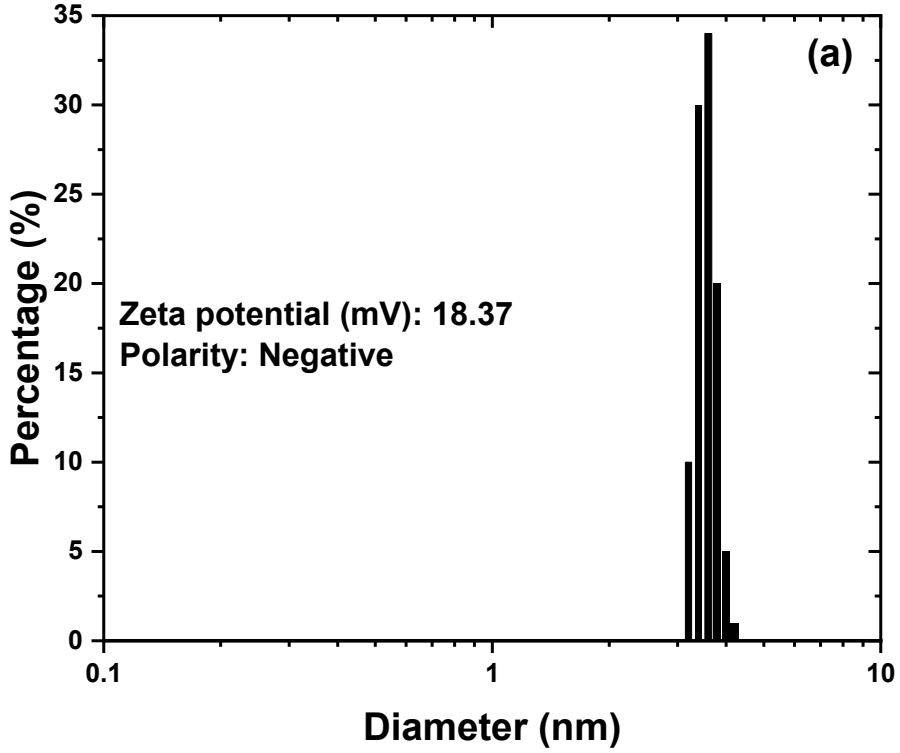
(a)
Zeta potential (mV): 18.37
Polarity: Negative
Percentage (%)
Diameter (nm)
0
5
10
15
20
25
30
35
0.1
1
10

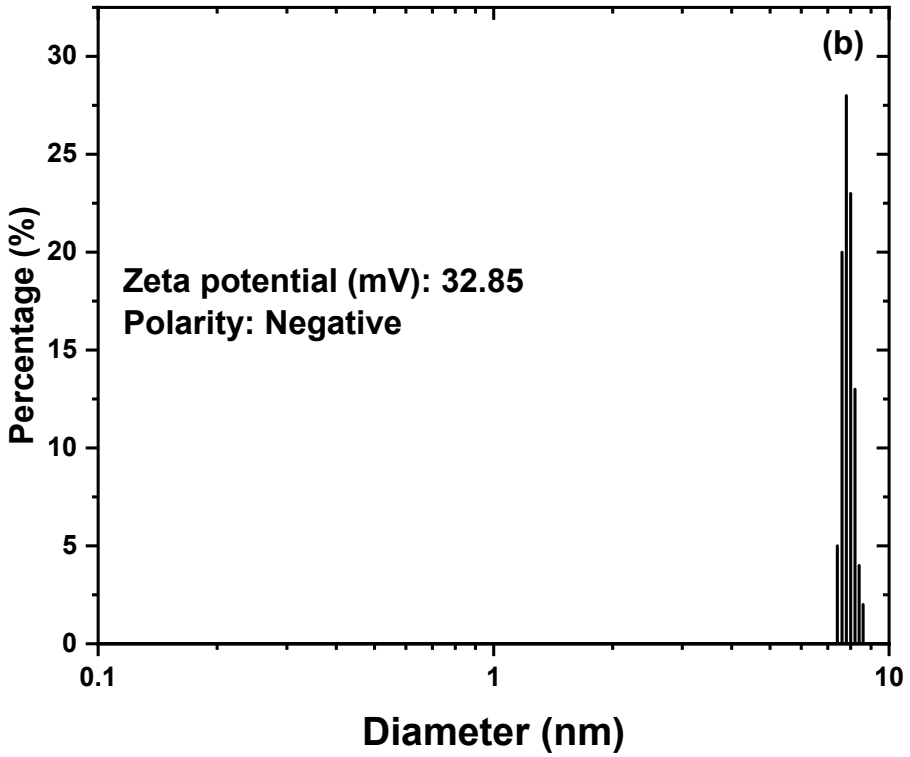
(b)
Zeta potential (mV): 32.85
Polarity: Negative
Percentage (%)
Diameter (nm)
0
5
10
15
20
25
30
0.1
1
10

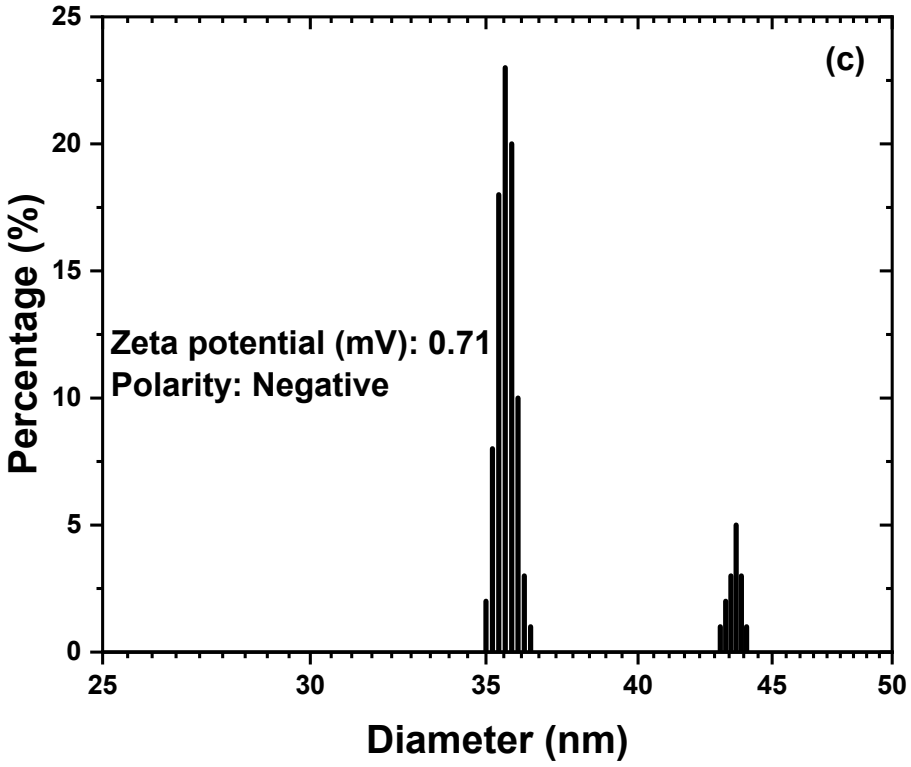

Figure S6. DLS analysis results for a) B-CQDs, b) G-CQDs, and C) WAG-CQDs, respectively.

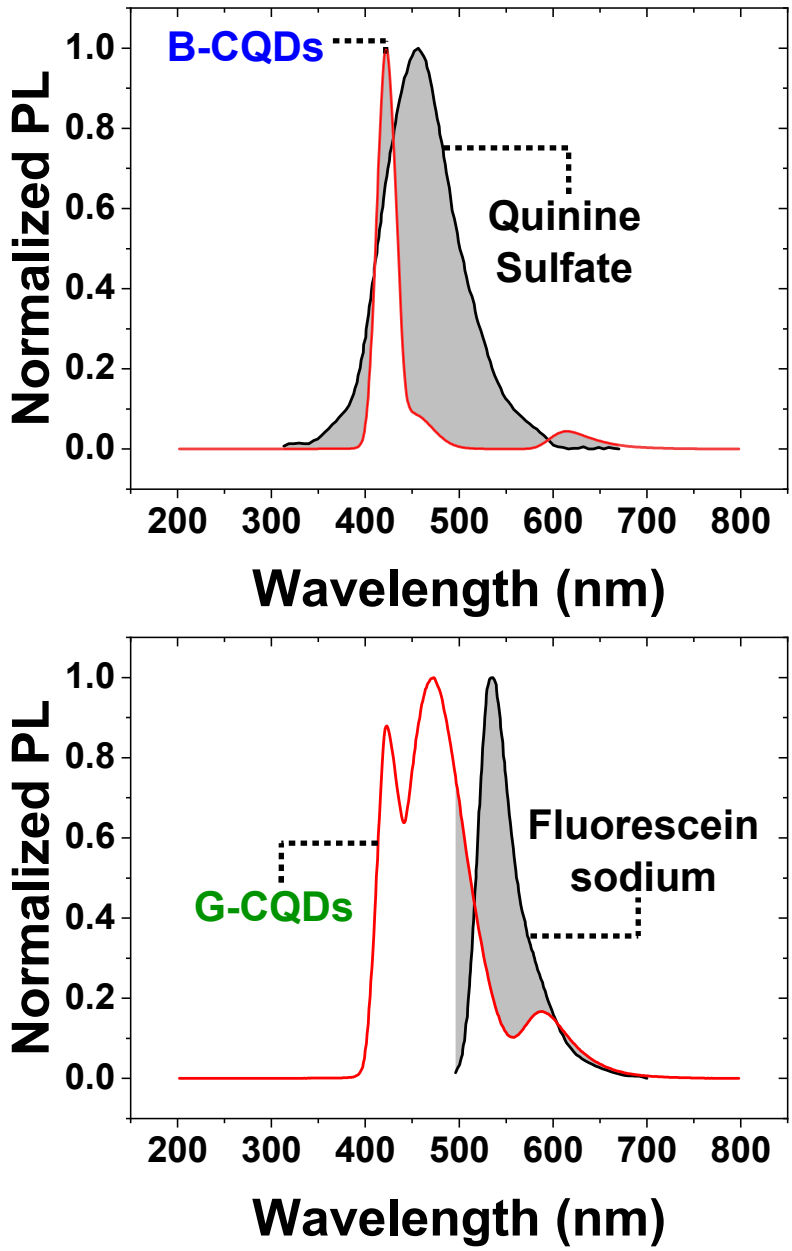

Figure S7. Normalized PL results to calculate PLQYs utilizing quinine sulfate and fluorescein sodium as the references.

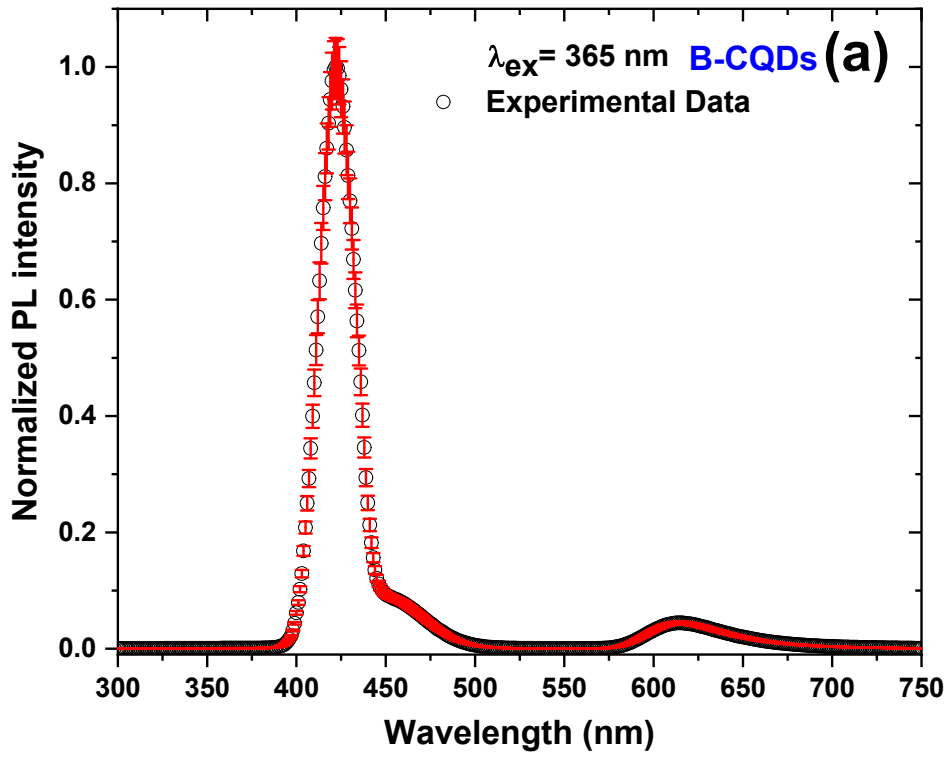
λex= 365 nm B-CQDs (a)
Experimental Data
Normalized PL intensity
Wavelength (nm)
0.0
0.2
0.4
0.6
0.8
1.0
300
350
400
450
500
550
600
650
700
750

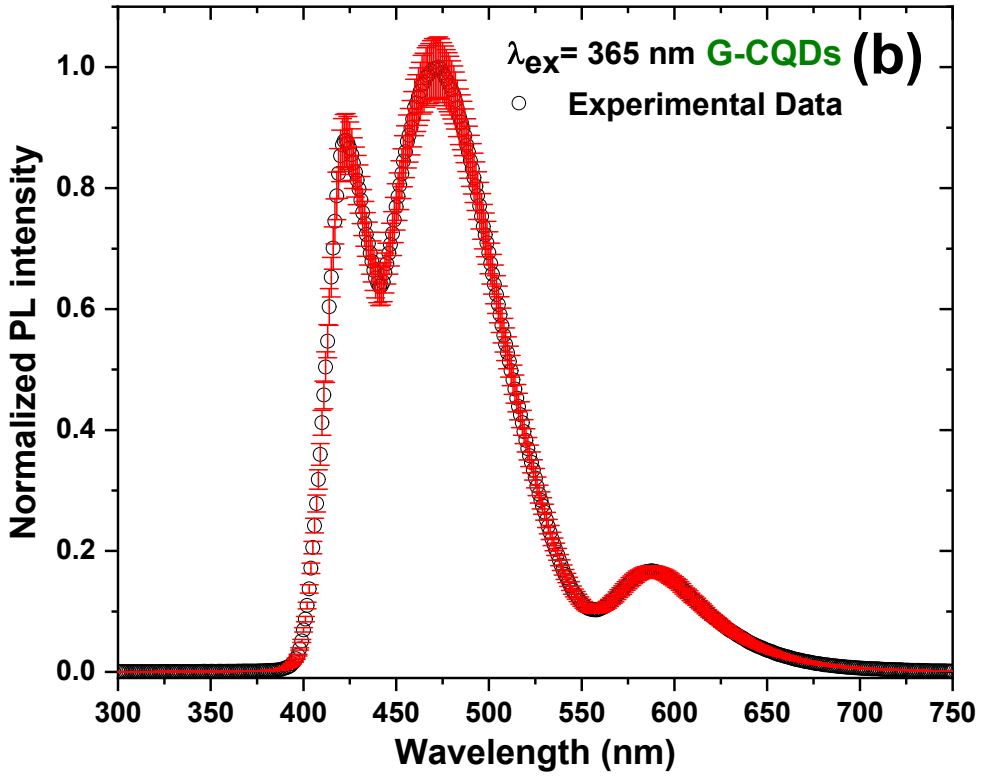
λex= 365 nm G-CQDs (b)
Experimental Data
Normalized PL intensity
Wavelength (nm)
0.0
0.2
0.4
0.6
0.8
1.0
300
350
400
450
500
550
600
650
700
750

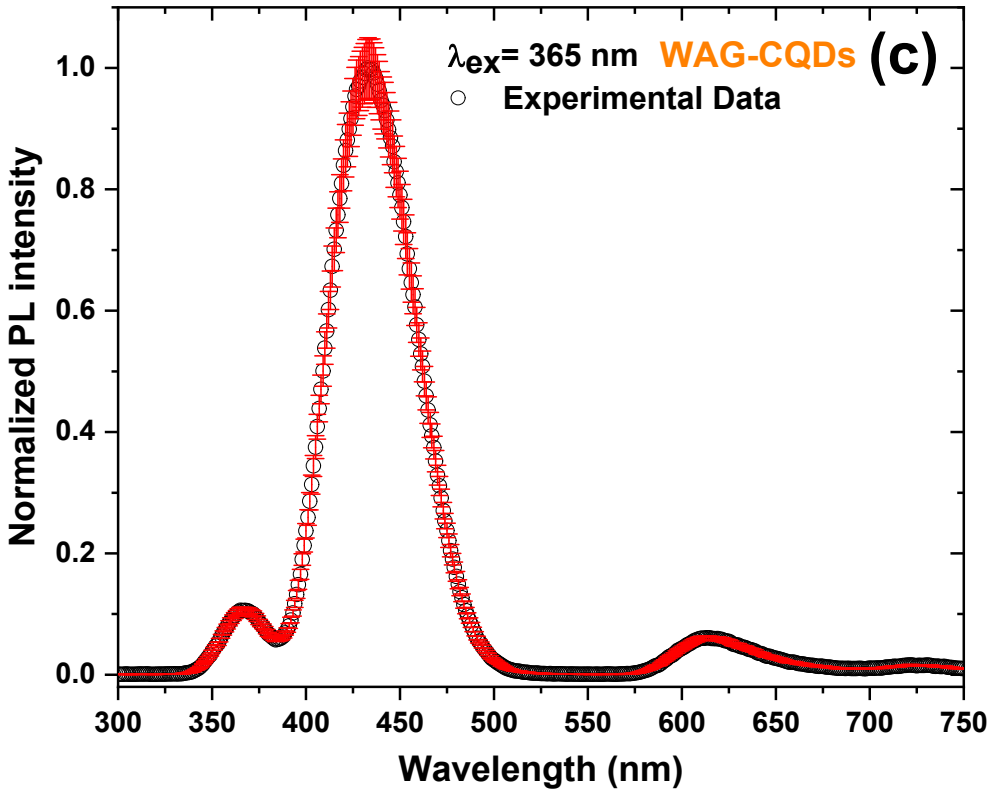

Figure S8. Calculated error bars for PL spectra of B-CQDs (a), G-CQDs (b), and WAG-CQDs (c)

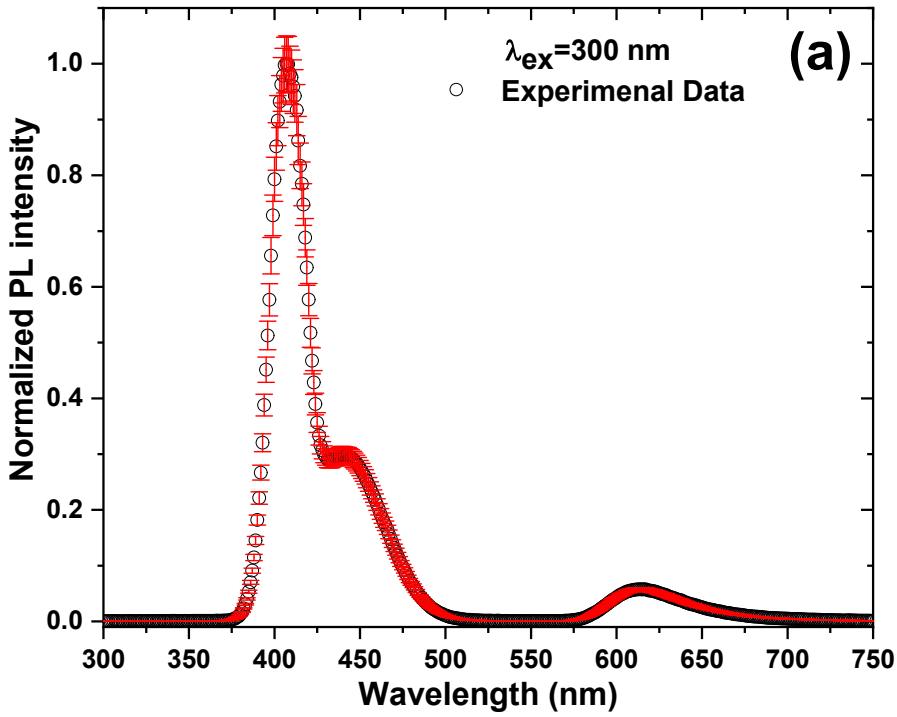

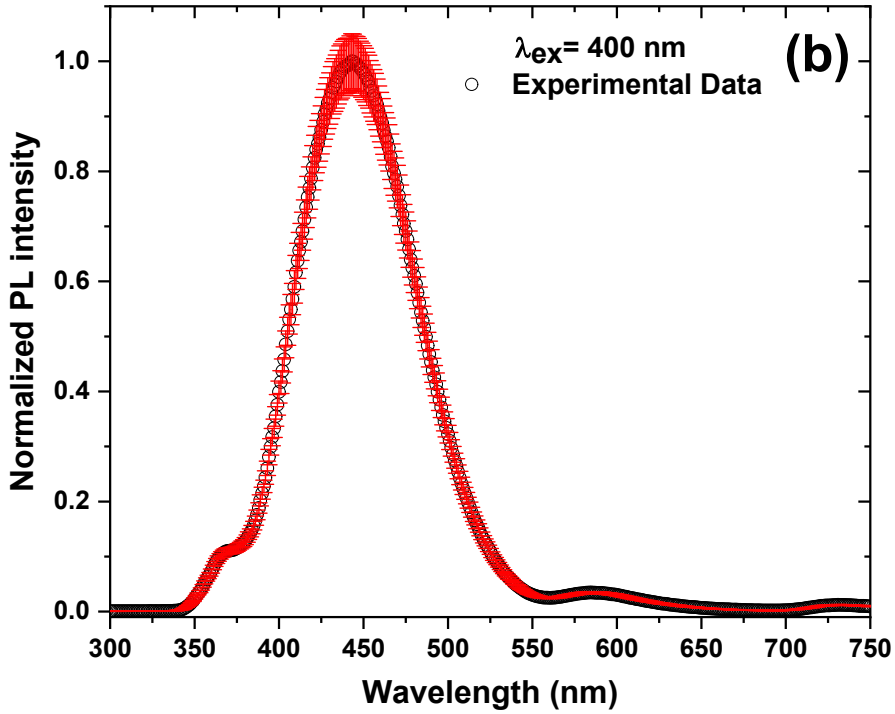

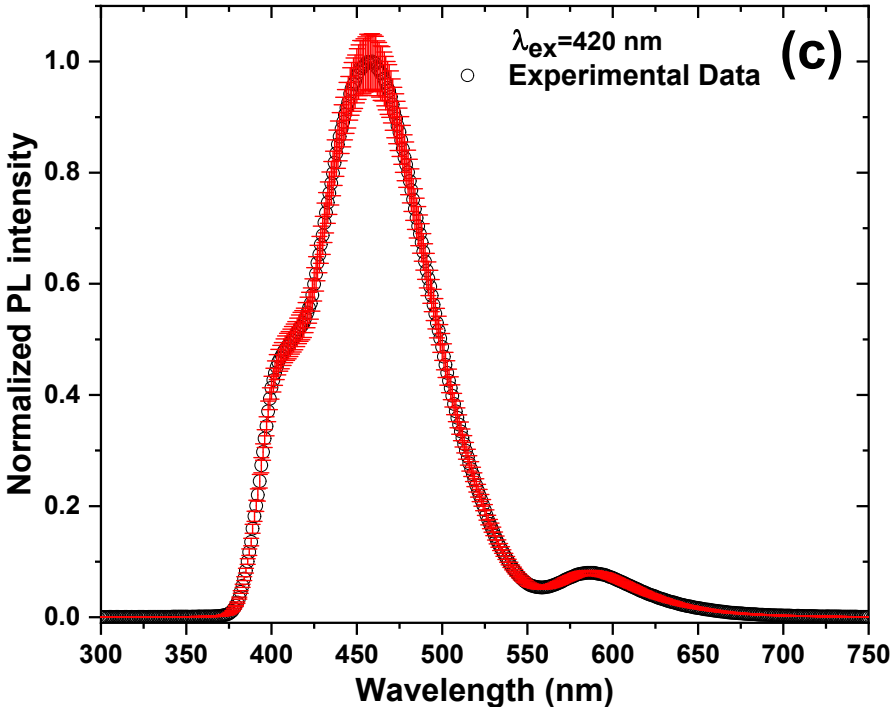

Figure S9. Calculated error bars for PL spectra of WAG-CQDs under 300nm (a), 365nm (b), 400nm (c), and 420nm (d) UV irradiation.

Reference

[1] M. Acik, G. Lee, C. Mattevi, A. Pirkle, R.M. Wallace, M. Chhowalla, K. Cho, Y. Chabal, The Role of Oxygen during Thermal Reduction of Graphene Oxide Studied by Infrared Absorption Spectroscopy, The Journal of Physical Chemistry C, 115 (2011) 19761-19781.
[2] A. Allahbakhsh, A.R. Bahramian, Self-assembly of graphene quantum dots into hydrogels and cryogels: Dynamic light scattering, UV–Vis spectroscopy and structural investigations, J. Mol. Liq., 265 (2018) 172-180.
[3] A. Allahbakhsh, F. Noei Khodabadi, F.S. Hosseini, A.H. Haghighi, 3-Aminopropyl-triethoxysilane-functionalized rice husk and rice husk ash reinforced polyamide 6/graphene oxide sustainable nanocomposites, European Polymer Journal, 94 (2017) 417-430.
[4] G. Kaur, M. Chaudhary, K.C. Jena, N. Singh, Terbium(iii)-coated carbon quantum dots for the detection of clomipramine through aggregation-induced emission from the analyte, New J. Chem., 44 (2020) 10536-10544.
[5] O. Masaru, S. Yuji, M. Hiromu, Molecular Vibrations and Force Fields of Alkyl Sulfides. IV. Infrared Spectra of Diethyl Sulfide, Bulletin of the Chemical Society of Japan, 45 (1972) 956-959.
[6] H. Michiro, S. Yuji, M. Hiromu, Molecular Vibrations and Structures of Polyalkyl Polysulfides. II. Polyethylene Disulfide, Bulletin of the Chemical Society of Japan, 39 (1966) 1861-1866.
[7] R. Souza da Costa, W. Ferreira da Cunha, N. Simenremis Pereira, A. Marti Ceschin, An Alternative Route to Obtain Carbon Quantum Dots from Photoluminescent Materials in Peat, Materials (Basel), 11 (2018) 1492.
[8] Z. Jiang, X. Zhao, Y. Fu, A. Manthiram, Composite membranes based on sulfonated poly(ether ether ketone) and SDBS-adsorbed graphene oxide for direct methanol fuel cells, Journal of Materials Chemistry, 22 (2012) 24862-24869.
[9] M. Acik, G. Lee, C. Mattevi, M. Chhowalla, K. Cho, Y.J. Chabal, Unusual infrared-absorption mechanism in thermally reduced graphene oxide, Nature Materials, 9 (2010) 840-845.
[10] A. Allahbakhsh, A.H. Haghighi, M. Sheydaei, Poly(ethylene trisulfide)/graphene oxide nanocomposites, Journal of Thermal Analysis and Calorimetry, 128 (2017) 427-442.
[11] R. Das, S. Parveen, A. Bora, P.K. Giri, Origin of high photoluminescence yield and high SERS sensitivity of nitrogen-doped graphene quantum dots, Carbon, 160 (2020) 273-286.
[12] B.A. Trofimov, L.M. Sinegovskaya, N.K. Gusarova, Vibrations of the S–S bond in elemental sulfur and organic polysulfides: a structural guide, Journal of Sulfur Chemistry, 30 (2009) 518-554.
[13] G. Rajender, P.K. Giri, Formation mechanism of graphene quantum dots and their edge state conversion probed by photoluminescence and Raman spectroscopy, J. Mater. Chem. C, 4 (2016) 10852-10865.